*applied sciences*

MDPI

*Article*

# Development and Validation of Accelerated Fretting Wear Test for Inconel 718 Against 304 Stainless Steel

**Bo Yang [1,2], Haitao Jiang [3], Xuexing Ding [3], Ying Luo [1,2] and Wenqiang Li [1,*]**

[1] School of Mechanical Engineering, Sichuan University, Chengdu 610065, China; npic007@163.com (B.Y.); drsiluo@163.com (Y.L.)
[2] National Key Laboratory of Nuclear Reactor Technology, Nuclear Power Institute of China, Chengdu 610041, China
[3] School of Petrochemical Engineering, Lanzhou University of Technology, Lanzhou 730050, China; 221080706002@lut.edu.cn (H.J.); dingxx1@163.com (X.D.)
* Correspondence: liwenqiang@scu.edu.cn@163.com

**Abstract**

Fretting wear significantly limits the service life of metal O-rings operating under harsh conditions. To address this limitation, this study investigates the wear behavior of metal O-rings under equivalent accelerated reciprocating motion and establishes an accelerated life prediction model based on similarity theory. Fretting wear experiments were conducted using Inconel 718 alloy and 304 stainless steel to replicate service conditions in a controlled laboratory environment. Wear morphology was characterized using laser scanning confocal microscopy, revealing a progressive transition from mild abrasive and adhesive wear to severe abrasive wear accompanied by material spalling. Based on the experimental results, regression analysis was performed to estimate the acceleration model coefficients, leading to the formulation of an equivalent acceleration equation capable of predicting seal wear life under practical service conditions. The resulting equivalent acceleration model can establish a quantitative connection between the acceleration test and the operating conditions. This model can shorten the testing time and can be used to predict parameters related to the surface morphology of static seals, providing a theoretical and experimental basis for reliable life assessment. This provides a practical basis for improving the reliability and safe operation of metal O-ring seals in critical applications, including nuclear energy and chemical processing systems.

**Keywords:** fretting wear; accelerated wear testing; Inconel 718 alloy; metal O-rings; similarity theory

Check for updates

Received: 18 March 2026
Revised: 20 April 2026
Accepted: 20 April 2026
Published: 23 April 2026

**Copyright:** © 2026 by the authors. Licensee MDPI, Basel, Switzerland. This article is an open access article distributed under the terms and conditions of the Creative Commons Attribution (CC BY) license.

## 1. Introduction

Metal O-rings are widely used for their reliable sealing performance in high-temperature, high-pressure, corrosive, and radioactive environments, making them critical components in the petroleum, chemical, aerospace, and nuclear energy industries [1–3]. Sealing in metal O-rings is achieved through elastoplastic deformation induced by initial interference or pre-compression, which fills microscopic surface defects, reduces leakage channels, and increases flow resistance [4]. Although seal replacement may be straightforward in some applications, most operating systems require shutdown and disassembly, resulting in substantial maintenance costs. Under harsh operating conditions, vibration and load fluctuations can induce progressive degradation at the sealing interface, among which fretting wear is a primary failure mechanism. Fretting wear is a form of accelerated

surface damage that occurs at the interface of contacting materials subjected to small-amplitude oscillatory motion, typically induced by mechanical vibration, load fluctuations, or differential thermal expansion of contacting surfaces [5].

In nuclear power systems, fretting wear has been extensively investigated in structural components such as alloy cladding tubes, steam generator tubes, fuel channels, and pressure pipes [6–13]. For example, Li et al. [14] investigated the fretting behavior of Zr-1Nb alloy cladding tubes under varying tangential displacement amplitudes and analyzed their effects on wear morphology, microstructure, and wear mechanisms. They found that increasing amplitude shifts the fretting regime from mixed to slip conditions. The friction coefficient initially increases and then decreases, while wear volume and depth increase progressively. The dominant wear mechanism transitions from adhesive wear to delamination wear, accompanied by intensified oxidation. Similarly, Lazarevic et al. [15] simulated grid–rod fretting in pressurized water reactors using a high-pressure test device and examined material combinations under high-temperature water environments. Winter et al. [16] compared the fretting performance of various cladding materials under high-temperature dry conditions and reported superior wear resistance of APMT steel relative to Zircaloy-4. The reported results provide data for evaluating the reliability of cladding materials under reactor operating conditions. In addition to these studies, Blaut [17] proposed a multi-stage engineering wear model for grid–rod fretting in nuclear fuel rods, incorporating environmental and material degradation effects during long-term operation. The model divides the wear process into an incubation stage, an oxide layer wear stage, and a matrix alloy wear stage, and accounts for complex factors such as high-temperature water environments, oxide layer phase transformation, and hydrogen embrittlement. The model predicts the evolution of wear depth in cladding tubes during long-term service.

In addition to structural components, fretting wear also affects sealing systems operating under similar harsh conditions. Zhang et al. [18] conducted experimental research on Inconel-based sealing systems for nuclear reactor pressure vessels. Their results showed that the friction coefficient increased with applied load. The SA508 surface exhibited material loss and oxidation of wear debris, whereas the Inconel 718 alloy underwent plastic deformation, forming a plastic flow layer that promoted adhesive wear. The dominant wear mechanism was identified as a combined effect of oxidative and abrasive wear. Zhang et al. [19] further investigated fretting damage in U–E type metal seals used in aerospace engines under high- and low-temperature as well as high-pressure conditions. The results showed that the friction coefficient increased rapidly during the initial stage and subsequently stabilized. During the reciprocating motion, the soft metal coating of the sealing lip transferred onto the flange surface. At elevated temperatures, plastic flow and oxidative wear were predominant, whereas brittle spalling dominated at low temperatures, significantly altering the surface morphology of the contact pair. Wang et al. [20] investigated the ball-end milled surface of Cr12MoV hardened die steel. By using finite element simulation and gray incidence analysis, they quantitatively analyzed the correlation between surface texture roughness parameters and wear volume per unit sliding distance, and developed a GM(0,6) prediction model for wear characteristics, which provides a novel approach for the wear resistance prediction of engineered surfaces with different topographies.

Despite existing studies, investigations specifically addressing the fretting wear behavior of metal O-ring seals during service remain limited. In pressure vessel sealing systems, vibration induced by load fluctuations frequently causes fretting damage at the sealing interface, which is often a primary contributor to seal failure. With increasingly demanding industrial operating conditions, requirements for long service life and high reliability have become more stringent. Accordingly, this study investigates the fretting characteristics and wear mechanisms of Inconel 718 and 304 stainless steel through controlled reciprocating

wear experiments. Based on similarity theory, an equivalent accelerated life prediction model is derived and calibrated using experimental data to establish a quantitative relationship between laboratory accelerated testing and service conditions. The results provide experimental evidence for understanding failure mechanisms in sealing systems and support reliability-oriented design and life assessment of metal O-ring sealing systems.

## 2. Equivalent Acceleration Model

Similarity theory provides a theoretical framework for experimental scaling analysis and has been widely applied in disciplines such as fluid mechanics, thermodynamics, and physical chemistry [21,22]. To establish a quantitative scaling relationship between laboratory accelerated testing and service wear behavior, dimensional analysis based on similarity theory and the Buckingham $\pi$ theorem is employed. The resulting similarity criterion expresses the functional relationship among the governing parameters of the wear process in dimensionless form, thereby capturing the coupled influence of multiple variables and enabling efficient organization of experimental data. To derive the similarity criterion for fretting friction and wear of metal O-rings [23–25], the following assumptions are introduced:

(1) Within the experimental range considered, the similarity relationship can be expressed in power-law form.

(2) Fretting wear is treated as dry sliding wear, and the test specimens adequately represent actual working conditions. Geometric and kinematic similarity requirements are satisfied.

(3) Within the selected test range, geometric parameters of the sealing component as well as material and environmental properties remain approximately constant; therefore, the corresponding dimensionless groups may be treated as constants.

Based on the $\pi$ theorem and the assumptions, the similarity criterion relationship for the metal O-ring friction and wear can be formulated as follows:

$$\begin{aligned} \prod_{\mathrm{ndi}} &= f_{\mathrm{i}}\left(\prod_{\mathrm{d1}}, \prod_{\mathrm{d2}}, \cdots, \prod_{\mathrm{dj}}\right) \\ &\approx \xi \prod_{\mathrm{d1}}^{\mathrm{n_1}} \prod_{\mathrm{d2}}^{\mathrm{n_2}} \cdots \prod_{\mathrm{dj}}^{\mathrm{n}_j} \\ &= \xi(\mathrm{Eu})^{n_1}\left(\frac{b_{\mathrm{f}}}{l}\right)^{n_2} \cdots \pi(\mathrm{Pr})^{n_{19}} \end{aligned} \tag{1}$$

where $\prod_{\mathrm{ndi}}$ (i = 1, 2, …, 10) represents quantitative similarity criteria; $j$ represents the number of qualitative similarity criteria, with $j$ = 19. The coefficients $\xi$ and $n_1 \sim n_{19}$ are constants whose values vary for different quantitative criteria. The dimensionless groups $\prod_{\mathrm{d1}} \sim \prod_{\mathrm{d19}}$ correspond to qualitative similarity criteria.

The independent dimensionless groups are defined as follows:

$$\begin{array}{llll} \prod_{\mathrm{nd1}} = \prod_{24} = f & \prod_{\mathrm{nd2}} = \prod_{25} = \frac{h}{l} & \prod_{\mathrm{nd3}} = \prod_{26} = \frac{A_{\mathrm{r}}}{A_{\mathrm{a}}} & \prod_{\mathrm{nd4}} = \prod_{27} = \frac{\rho V Q}{F_{\mathrm{g}}} \\ \prod_{\mathrm{nd5}} = \prod_{28} = K_{\mathrm{v}} & \prod_{\mathrm{nd6}} = \prod_{29} = \mathrm{Nu} & \prod_{\mathrm{nd7}} = \prod_{12} = B & \prod_{\mathrm{nd8}} = \prod_{18} = \frac{\theta_f}{\Delta\theta} \\ \prod_{\mathrm{nd9}} = \prod_{4} = \frac{R_{D\tau}}{l} & \prod_{\mathrm{nd10}} = \prod_{5} = \frac{R_{D\mathrm{st}}}{R_{D\tau}} & & \end{array}$$

where $h$ is film thickness within the interface; $l$ is the characteristic dimension; $A_{\mathrm{r}}$ is the true contact area; $A_{\mathrm{a}}$ is the nominal contact area; $\rho$ is the density of sealed medium; $V$ is the sliding velocity; $Q$ is the leakage rate; $F_{\mathrm{g}}$ is the total load on the end face; $K_{\mathrm{v}}$ is the wear rate; Nu is the Nusselt number; $\theta_f$ is the medium temperature within the interface; and $\Delta\theta$ is the allowable temperature difference.

Noting that the qualitative similarity criteria, $\prod_2$, $\prod_6 \sim \prod_{11}$, $\prod_{13} \sim \prod_{17}$ and $\prod_{19}$, consist solely of geometric parameters and material properties, and remain invariant within the selected experimental range; the power-law contributions of 13 of the 19 qualitative

similarity criteria may therefore be absorbed into constant coefficients. Consequently, Equation (1) can be simplified to:

$$\begin{aligned}\Pi_{\mathrm{ndi}} &= C_0 \mathrm{Eu}^{n_1} {\varepsilon_1}^{n_2} \hat{G}^{n_3} \mathrm{Re}^{n_4} \mathrm{Pe}^{n_5} \mathrm{Pr}^{n_6} \\ &= C_0 \left(\frac{\Delta p}{V^2 \rho}\right)^{n_1} \left(\frac{p_g}{E_1}\right)^{n_2} \left(\frac{\eta V b_f}{F_g}\right)^{n_3} \left(\frac{Vl\rho}{\eta}\right)^{n_4} \left(\frac{\rho c_s V l}{\lambda_s}\right)^{n_5} \left(\frac{\mathrm{Pr}}{\lambda_s}\right)^{n_6}\end{aligned} \tag{2}$$

In this expression, $C_0$, $n_1 \sim n_6$ are constants, and their values are different for different $\prod_{\mathrm{ndi}}$.

To derive a closed-form empirical expression for the similarity relationship, additional simplifying assumptions are introduced. The influence of strain on the wear response is considered negligible within the experimental range, and the temperature difference between the sealing end faces is assumed to be small under normal operating conditions. Consequently, temperature-dependent variations in material properties and transport parameters may be neglected. In particular, the Prandtl number Pr, which depends on the viscosity of the medium and is sensitive to temperature, can be treated as approximately constant. Under these conditions, and in conjunction with similarity theory, the governing similarity criterion for fretting wear may be derived. Considering that the strain and temperature variations remain negligible during frictional contact, the similarity relationship can be further reduced to the following simplified form:

$$\begin{aligned}\pi_i &= C' V^{n_1} \mathrm{Eu}^{n_2} \hat{G}^{n_3} \\ &= C' V^{n_1} \left(\frac{\Delta p}{V^2 \rho}\right)^{n_2} \left(\frac{\eta V b}{F_g}\right)^{n_3}\end{aligned} \tag{3}$$

where $C'$ represents dimensional undetermined coefficients associated with the sealing material and medium properties, while $\mathrm{n}_1$, $\mathrm{n}_2$, and $\mathrm{n}_3$ are undetermined exponents. According to Equation (3), the similarity relationship may be written as:

$$\pi_{\mathrm{nd3}} = C_3' V^{x_1} \mathrm{Eu}^{x_2} \hat{G}^{x_3} = C_3' V^{x_1} \left(\frac{\Delta p}{V^2 \rho}\right)^{x_2} \left(\frac{\eta V b_f}{F_g}\right)^{x_3} \tag{4}$$

$$\pi_{\mathrm{nd3}} = C_5' V^{y_1} \mathrm{Eu}^{y_2} \hat{G}^{y_3} = C_3' V^{y_1} \left(\frac{\Delta p}{V^2 \rho}\right)^{y_2} \left(\frac{\eta V b_f}{F_g}\right)^{y_3} \tag{5}$$

Here, $C_3'$ and $C_5'$ are dimensional undetermined coefficients. Dividing Equation (4) by Equation (5) yields:

$$\begin{aligned}\frac{\pi_{\mathrm{nd3}}}{\pi_{\mathrm{nd5}}} &= \frac{{A_r}^*}{K_v} = \frac{C_3'}{C_5'} V^{x_1 - y_1} \mathrm{Eu}^{x_2 - y_2} \hat{G}^{x_3 - y_3} \\ &= \frac{C_3'}{C_5'} V^{x_1 - y_1} \left(\frac{\Delta p}{V^2 \rho}\right)^{x_2 - y_2} \left(\frac{\eta V b_f}{F_g}\right)^{x_3 - y_3}\end{aligned} \tag{6}$$

This can be expressed equivalently as:

$$\begin{aligned}{A_r}^* &= \frac{C_3'}{C_5'} V^{x_1 - y_1} \left(\frac{\Delta p}{V^2 \rho}\right)^{x_2 - y_2} \left(\frac{\eta V b_f}{F_g}\right)^{x_3 - y_3} K_v \\ &= C'' V^{x_1 - y_1} \left(\frac{\Delta p}{V^2 \rho}\right)^{x_2 - y_2} \left(\frac{\eta V b_f}{F_g}\right)^{x_3 - y_3} \frac{V_F H}{p_g V} \\ &= C'' V^{z_1} \left(\frac{\Delta p}{V^2 \rho}\right)^{z_2} \left(\frac{\eta V b_f}{F_g}\right)^{z_3} \frac{H}{p_g} \frac{\delta_t}{t}\end{aligned} \tag{7}$$

In the expression, ${A_r}^*$ is the ratio of the actual contact area to the nominal contact area, i.e., ${A_r}^* = A_r / A_a$. The coefficient $C''$ depends on the sealing material and the medium properties; $\delta_t$ is the wear amount, $t$ is the time (s), and $z_1$, $z_2$, $z_3$ are undetermined exponents.

During wear, the surface morphology of the test specimen changes over time. By incorporating a time term into contact theory, the relationship between fractal parameters and time is obtained. Considering the relationship between contact surface degradation and leakage behavior, a wear-accelerated life prediction model is formulated to characterize the

progressive deterioration of the sealing interface. The resulting time-dependent expression for the contact surface parameters is given as follows:

$$\begin{cases} A_r = A_a A_r^* \left( p_g, C^*, a_c^*, a_{pe}^*, E, K, \varphi \right) \\ A_r^* = C'' v^{z_1} \left( \frac{\Delta p}{v^2 \rho} \right)^{z_2} \left( \frac{\eta v b}{F_g} \right)^{z_3} \frac{H}{p_g} \frac{\delta_t}{t} \end{cases} \tag{8}$$

Under conditions where other governing parameters remain constant, a unique correspondence exists between the cavity area and the leakage rate. When a specified leakage threshold is reached, the sealing end faces exhibit an identical wear amount and an equivalent cavity area. However, the time required to attain a given cavity area varies with operating conditions. This time dependence provides the basis for establishing an equivalence relationship between service conditions and accelerated testing. Accordingly, the accelerated life test model for the metal O-ring sealing end face, formulated based on fractal theory, is expressed as follows:

$$\frac{t_2}{t_1} = \frac{v_2^{z_1}}{v_1^{z_1}} \left( \frac{Eu_2}{Eu_1} \right)^{z_2} \left( \frac{\hat{G}_2}{\hat{G}_1} \right)^{z_3} \frac{\delta_{t2}}{\delta_{t1}} \frac{p_{g1}}{p_{g2}} \tag{9}$$

The above expression represents an accelerated wear test model for the metal O-ring sealing end face derived from fractal theory. By measuring the wear amount δt1 under simulated working condition 1 for a duration t1, the equivalent time t2 required to produce a wear amount δt2 under real working conditions, corresponding to the same end-face characteristic roughness, can be determined.

## 3. Experimental Materials and Procedures

### *3.1. Test Materials Specification*

Inconel 718 alloy and 304 stainless steel were selected as the test materials to represent the sealing pair. The upper specimen was fabricated from Inconel 718, while the lower specimen was manufactured from 304 stainless steel. The upper specimen measured $\Phi 6 \times 7$ mm, and the lower specimen measures $\Phi 19 \times 8$ mm, as shown in Figure 1. The mechanical properties of the materials are summarized in Table 1. The chemical compositions of Inconel 718 and 304 stainless steel materials are respectively shown in Tables 2 and 3. Before the experiment, the surface of the specimen was polished using a metallographic polishing machine. The specimen was then ultrasonically cleaned and dried with acetone solution. The surface morphology of the specimen was measured. The roughness of both the upper test sample and the lower test part was 0.2 μm. Before the experiment, the specimen was again ultrasonically cleaned and dried.

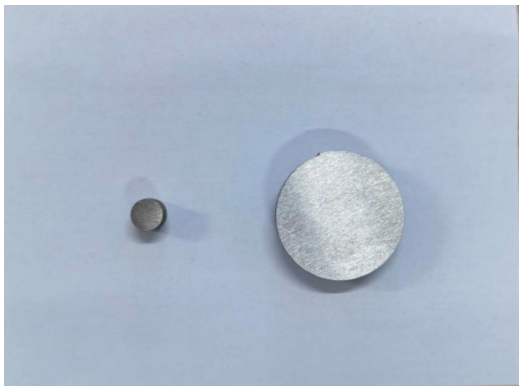


**Figure 1.** Photograph of the upper and lower test specimens used in the fretting wear experiments.

**Table 1.** Mechanical properties of test materials.

| Material Parameter | Inconel 718 | 304 Stainless Steel |
|---|---|---|
| Elastic modulus/MPa | 213,000 | 200,000 |
| Poisson's ratio | 0.3 | 0.3 |
| Yield strength/MPa | 1087 | 287 |

**Table 2.** Chemical compositions of Inconel 718.

| Element | Ni | Cr | Nb | Ta | Mo | Ti | Co | Mn | Si |
|---|---|---|---|---|---|---|---|---|---|
| Content | 52.62 | 18.80 | 5.07 | <0.002 | 3.00 | 0.88 | 0.14 | 0.029 | 0.072 |
| Element | Cu | C | S | Al | B | P | Fe | Pb | |
| Content | 0.11 | 0.049 | 0.001 | 0.39 | 0.0036 | 0.003 | 18.33 | 0.00005 | |

**Table 3.** Chemical precent compositions of 304 stainless steel.

| Element | C | Si | Mn | P | S | Cr | Ni | N |
|---|---|---|---|---|---|---|---|---|
| Content | 0.03 | 0.50 | 1.05 | 0.029 | 0.002 | 18.09 | 8.03 | 0.04 |

### *3.2. Specimen Preparation and Characterization*

Surface contaminants were removed by ultrasonic cleaning in acetone. The contact surfaces were subsequently ground using progressively finer abrasive papers and polished with a metallographic polishing system until no visible scratches remained, ensuring approximately uniform surface roughness. The specimens were then ultrasonically cleaned again in acetone and air-dried.

Surface morphology was characterized before and after wear testing using an OLYMPUS 5000 laser scanning confocal microscope (Tokyo, Japan). The mass of each specimen was measured using a METTLER TOLEDO (Zurich, Switzerland) analytical balance before and following testing, and wear was quantified based on mass loss.

### *3.3. Fretting Wear Test Procedure*

Fretting wear experiments were conducted using an Rtec MFT-5000 tribometer (Aubel, Switzerland), as shown in Figure 2. The system comprises a computer-controlled loading unit, an XY bidirectional stage, force sensors, and an environmental test chamber. All experimental data, including friction force and displacement, were automatically acquired and recorded for subsequent analysis. The entire testing cycle was controlled by software and could be adjusted according to specific requirements.

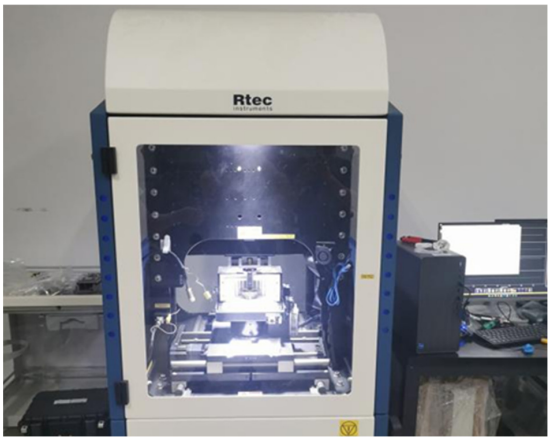



**Figure 2.** Rtec MFT-5000 fretting wear testing system.

The test parameters for fretting wear were set as follows: normal load Fn = 111 N, displacement amplitude was 600 μm, frequency of 45 Hz, and test duration of 12 h. All experiments were performed at ambient temperature (20–25 °C). During the test, the upper Inconel 718 specimen was fixed in the loading position, while the lower 304 stainless steel specimen was moved horizontally.

## 4. Experimental Results and Analysis

### 4.1. Changes in Fractal Parameters of Sealing End Face with Wear Time

The evolution of the fractal dimension $D$ and the fractal roughness parameter $G$ with wear time was determined using the structure function method [26] based on surface profiles of the 304 stainless steel specimen, measured by the OLYMPUS 5000 laser scanning confocal microscope. Figures 3 and 4 present the variation in $D$ and $G$ as a function of wear time, respectively.

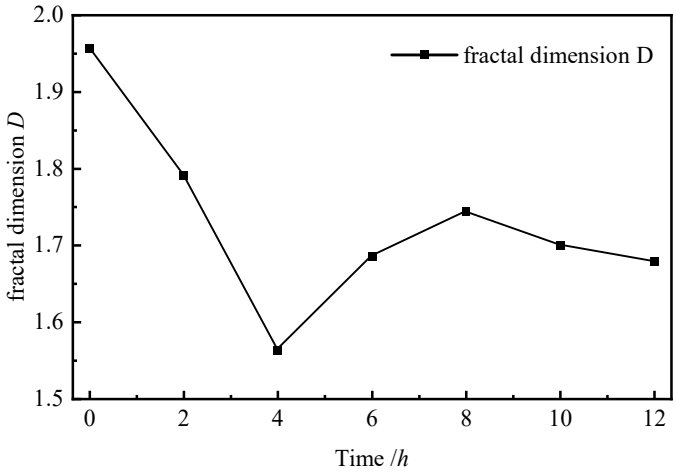



**Figure 3.** Change in fractal dimension $D$ with wear time.

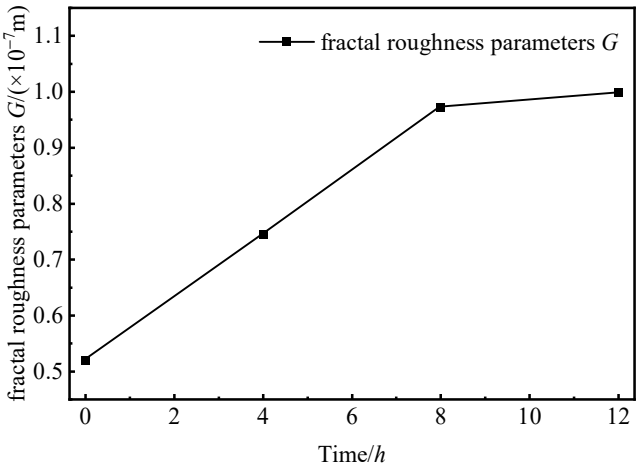



**Figure 4.** Variation in fractal roughness parameters $G$ with wear time.

The experimental results indicate that $D$ and $G$ of the 304 stainless steel sealing end face exhibit a clear inverse evolutionary trend during the fretting wear process. As shown in Figure 4, the fractal dimension is relatively high in the initial stage of wear, then decreases progressively with increasing wear time, and gradually approaches a stable value at the later stage. This behavior suggests that, at the onset of friction, the surface retains multi-scale asperity features originating from the initial machining process, resulting in a relatively less complex and smoother topography. As wear proceeds, prominent asperity peaks are

progressively sheared off, fractured, and detached, leading to the reorganization of surface features and a reduction in fractal complexity, which is reflected by the decrease in $D$. In contrast, $G$ increases overall with wear time and eventually stabilizes, as shown in Figure 4. During the early stage of wear, the surface is dominated by fine, densely distributed micro-asperities. With continued sliding, small-scale asperities are gradually removed, while larger-scale features such as wear grooves, plastic flow regions, and localized spalling pits become more pronounced. This transition toward larger characteristic surface features results in an increase in the representative scale parameter $G$. Once the wear process reaches a quasi-steady state, the rate of morphological evolution diminishes, and the variation in $G$ correspondingly becomes less significant.

By regressing the experimental data, the equations relating $D$-$t$ and $G$-$t$($R^2$ = 0.92), as shown in Equations (10) and (11), were obtained, respectively:

$$D(t) = \begin{cases} -0.2784t + 1.7601 & 0 < t < 4 \\ 0.1275t + 1.6534 & 4 < t < 8 \\ -0.046t + 1.7109 & 8 < t < 12 \end{cases} \quad (10)$$

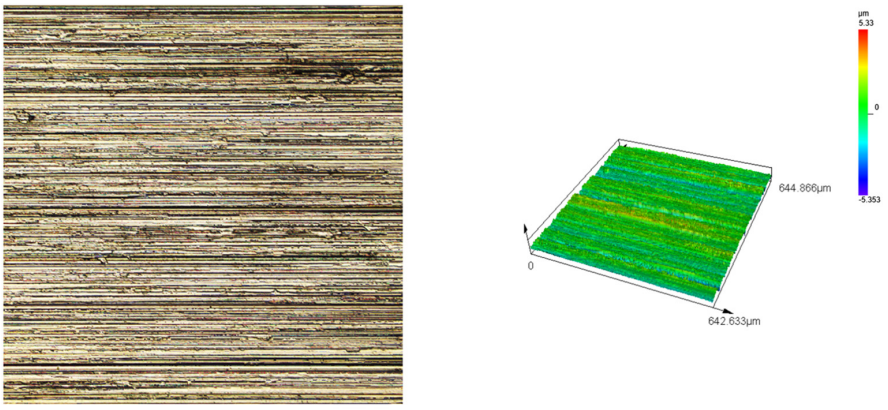
$$G(t) = (0.4125t + 5.5960) \times 10^{-8} \; 0 < t < 12 \quad (11)$$

Based on the above relational equations, the fractal dimension and fractal roughness parameters of the rough surface during the wear process can be predicted.

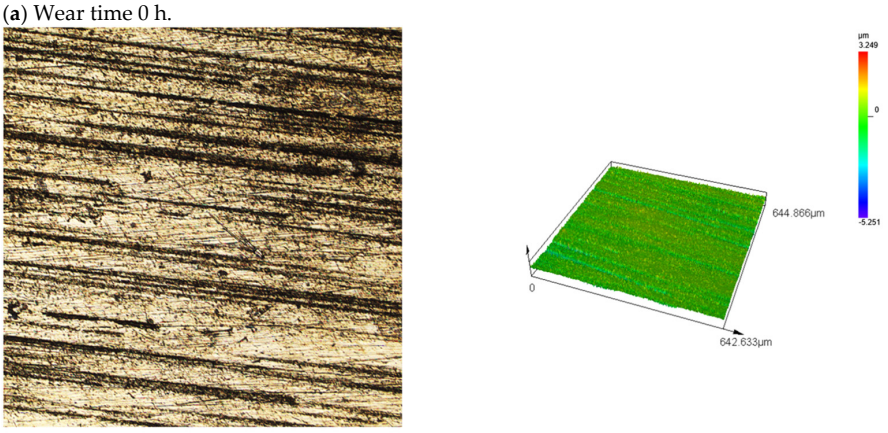
### 4.2. Wear Morphology and Mechanism Analysis

The surface morphology was analyzed to elucidate the evolution of wear mechanisms with increasing fretting duration. The morphological evolution of the Inconel 718 and 304 stainless steel surfaces, together with their three-dimensional topographical reconstruction, is presented in Figures 5 and 6. Based on these two-dimensional surface profiles and three-dimensional topographical analyses of the worn surfaces, the fretting wear mechanisms of 304 stainless steel were systematically compared and discussed at different stages of wear.

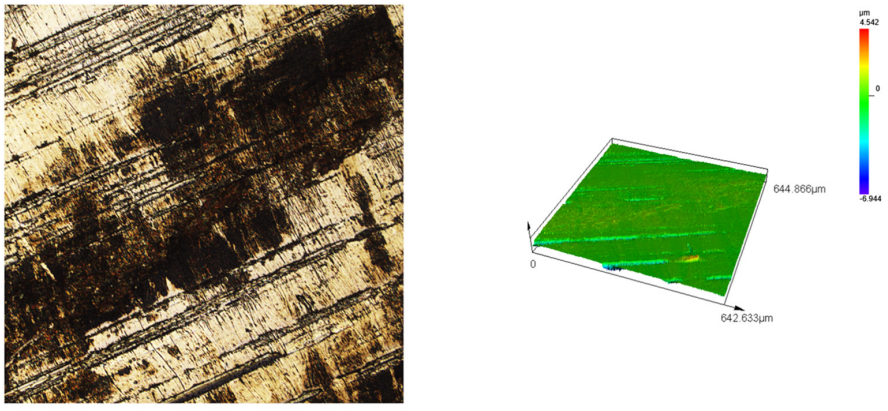
Based on the surface morphology images and corresponding 3D morphology, the wear morphology exhibits a clear stage-dependent evolution with increasing wear time. The unworn surface is relatively smooth, retaining only the original machining texture, and the 3D morphology reveals minimal asperity height variation, indicating minimal material damage. After 4 h of fretting, localized darkened regions and fine scratches emerge, especially concentrated within the contact zone. The 3D reconstruction displays moderately increased asperity heights, consistent with the onset of mild abrasive wear accompanied by initial adhesive interactions. At 8 h, the wear scar expands markedly, and numerous furrows, spalling pits, and debris accumulations become evident. The corresponding 3D morphology demonstrates significantly amplified asperity height variations, indicating a transition to a moderate wear regime governed by the combined action of abrasive and adhesive mechanisms. When the wear duration reaches 12 h, the damaged region extends across nearly the entire contact area. Pronounced grooves, material spalling, and heterogeneous debris accumulation are observed. The 3D morphology shows significant asperity height differences, confirming the development of a severe wear stage dominated by intensified abrasive and adhesive wear. Overall, the surface degradation progresses systematically from mild to severe with increasing wear time, accompanied by continuous amplification of morphological damage.



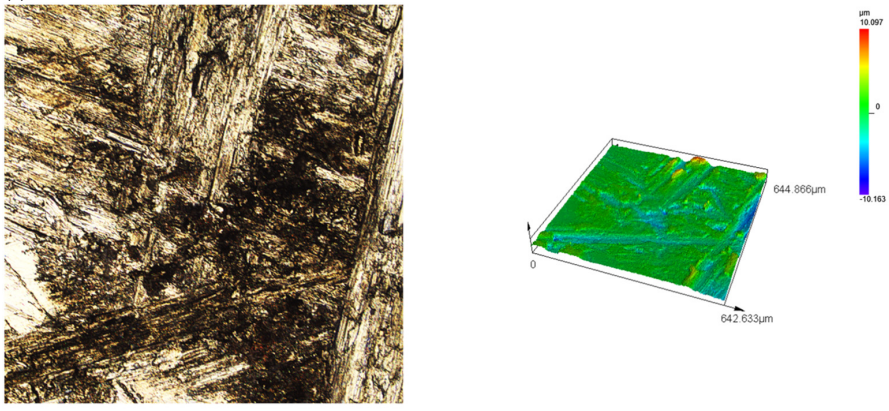

(**a**) Wear time 0 h.




(**b**) Wear time 4 h.

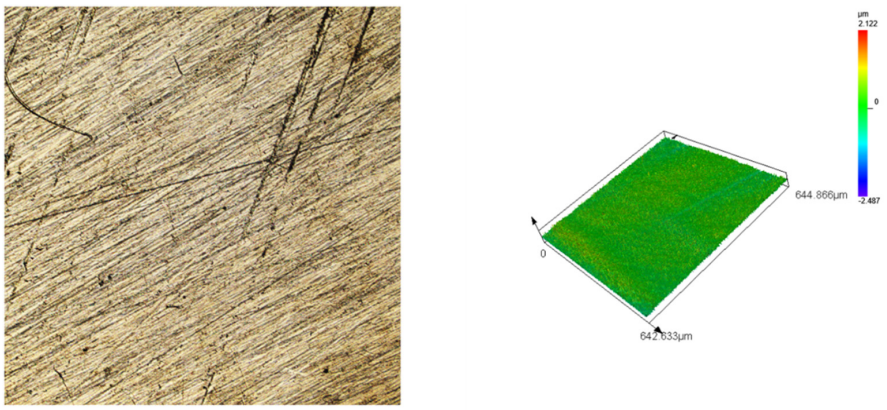



(**c**) Wear time 8 h.

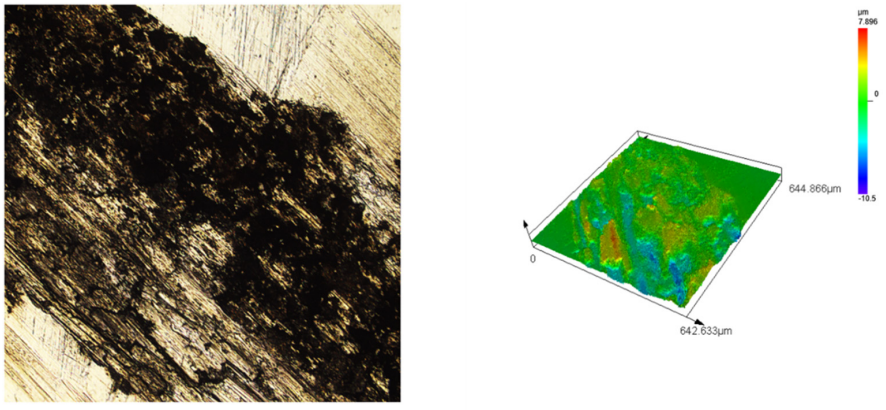



(**d**) Wear time 12 h.

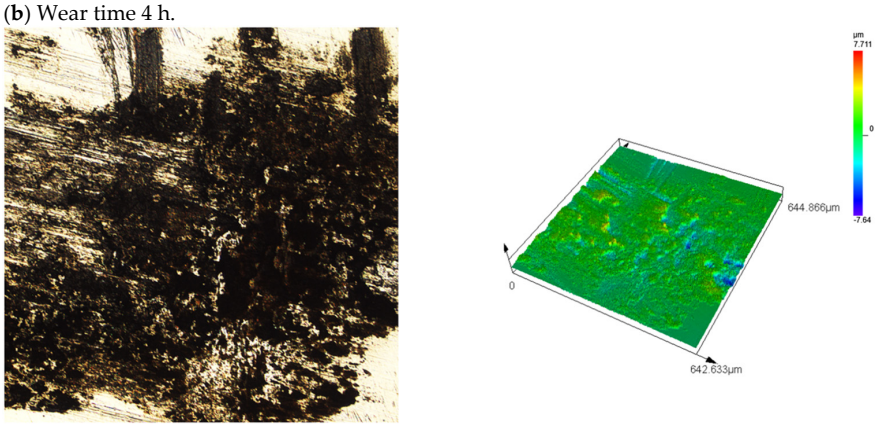
**Figure 5.** Surface morphology of Inconel 718 at different wear times (0–12 h): optical images (**left**) and corresponding three-dimensional topographical reconstructions (**right**).



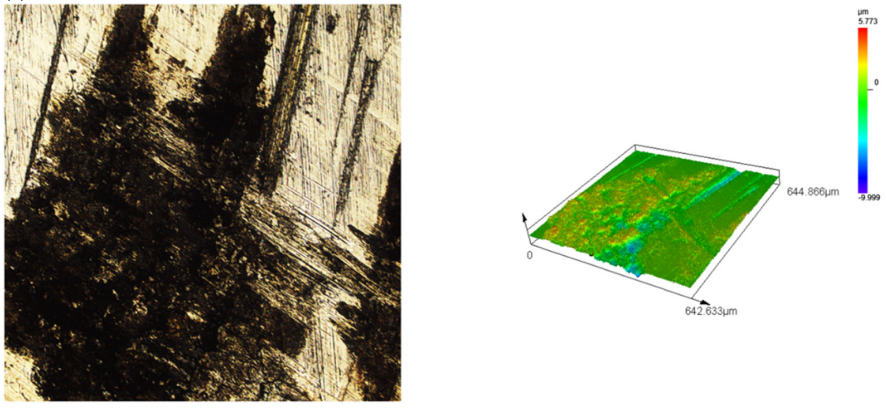

(**a**) Wear time 0 h.




(**b**) Wear time 4 h.




(**c**) Wear time 8 h.




(**d**) Wear time 12 h.

**Figure 6.** Surface morphology of 304 stainless steel at different wear times (0–12 h): optical images (**left**) and corresponding three-dimensional topographical reconstructions (**right**).

## 5. Determination and Verification of Undetermined Coefficients in the Equivalent Accelerated Life Model

Based on the equivalent accelerated life model for fretting wear derived in Section 2, the service wear time can be effectively shortened in laboratory experiments by increasing the applied normal load and reciprocating velocity at the sealing interface. By substituting $E_u = \Delta p / V^2 \rho$ and $\hat{G} = \eta v b_f / F_g$ into the similarity criterion equation, a simplified accelerated friction–wear model is obtained, as expressed in Equation (12).

$$\frac{t_2}{t_1} = \left(\frac{v_2}{v_1}\right)^{Z_1 - 2Z_2 + Z_3} \left(\frac{p_{g1}}{p_{g2}}\right)^{Z_3+1} \frac{\delta_{t_2}}{\delta_{t_1}} \tag{12}$$

From Equation (12), by selecting different combinations of p and v, the exponents $Z_1$, $Z_2$, and $Z_3$ can be determined. Defining $Z_1 - 2Z_2 = Z_{12}$, Equation (12) can be rewritten as:

$$\frac{t_2}{t_1} = \left(\frac{v_2}{v_1}\right)^{Z_{12} + Z_3} \left(\frac{p_{g1}}{p_{g2}}\right)^{Z_3+1} \frac{\delta_{t_2}}{\delta_{t_1}} \tag{13}$$

To identify the unknown coefficients, multiple parallel experiments were conducted. Experimental datasets exhibiting consistent wear trends were selected for subsequent parameter fitting and analysis. Through iterative testing and result analysis, the representative operating conditions summarized in Table 4 were determined.

**Table 4.** Experimental data under three different wear conditions.

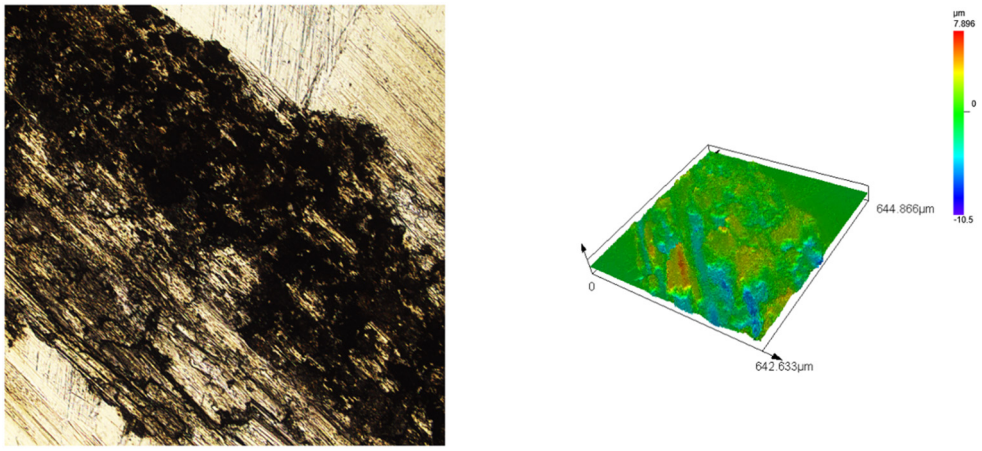
| Operating Conditions | Load/N | Frequency/Hz | Displacement Amplitude/μm | Wear Time/h | Cumulative Wear |
|---|---|---|---|---|---|
| 1 | 111 | 45 | 600 | 12 h | 0.15 |
| 2 | 84 | 60 | 600 | 12 h | 0.17 |
| 3 | 94 | 53 | 600 | 12 h | 0.15 |

By substituting the wear data obtained under the three operating conditions into Equation (13), the fitted exponents were determined as $Z_{12} = -16.6209$ and $Z_3 = 8.2369$.

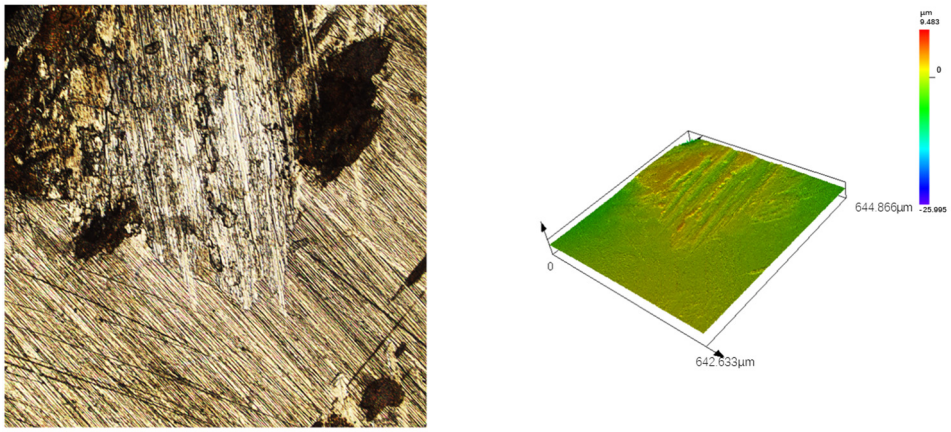
To further validate the proposed equivalent accelerated life model, an additional verification test (operating condition 4) was conducted under a normal load of 107 N, a displacement amplitude of 600 μm, a frequency of 43 Hz, and a test duration of 8.2 h. The results were compared with those obtained under operating condition 1 (111 N, 600 μm, 45 Hz, 4 h). The resulting surface morphologies and corresponding two-dimensional profiles are shown in Figures 7 and 8, respectively. The extracted fractal parameters were used to quantify surface evolution under both conditions. The relative errors of wear amount, fractal dimension, and fractal roughness parameters are shown in Table 5. All deviations are within 20%, indicating satisfactory agreement between the predictions of the equivalent accelerated life model and experimental results.

**Table 5.** Comparison of test results.

| Test Results | Condition 1 | Condition 4 | Relative Error |
|---|---|---|---|
| Wear amount/mg | 0.09 | 0.08 | 11.1% |
| Fractal dimension | 1.6032 | 1.6647 | 3.8% |
| Fractal roughness parameters/m | $5.0823 \times 10^{-8}$ | $4.2064 \times 10^{-8}$ | 17.2% |




(**a**) Condition 1: Wear time 4 h.




(**b**) Condition 4: Wear time 8.2 h.

**Figure 7.** Comparison of surface morphology after wear under operating conditions 1 and 4.

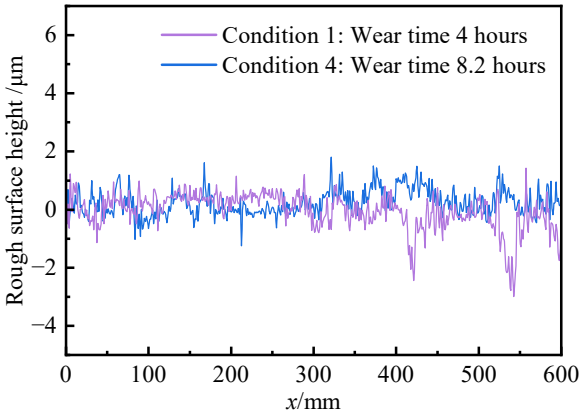



**Figure 8.** Two-dimensional profile curves of the surface roughness after wear under operating conditions 1 and 4.

## 6. Conclusions

Fretting wear experiments under room temperature were performed on an Inconel 718 and 304 stainless steel sealing pair representative of nuclear reactor pressure vessel sealing interfaces. The friction response under different normal loads was analyzed, and the corresponding wear morphology and mechanisms were identified. An equivalent accelerated life model was further established based on similarity theory and calibrated using experimental data. The main conclusions are as follows:

(1) During fretting, the 304 stainless steel surface developed a plastic flow layer and exhibited friction-induced oxidation. The dominant wear behavior is attributable to the combined action of adhesive wear, abrasive wear, and oxidative wear.

(2) Fretting at the interface between Inconel 718 alloy and 304 stainless steel produced surface defects, including wear scars and associated damage features, which can degrade sealing integrity and increase the risk of leakage. These friction and wear effects should therefore be explicitly considered in the design and reliability assessment of sealing interfaces in reactor systems.

(3) An accelerated testing methodology for sealing end face wear was developed using similarity theory, enabling systematic shortening of test duration via controlled changes in operating parameters. The wear evolution with time was quantified experimentally, and regression analysis was used to identify the undetermined model constants and exponents. The resulting equivalent accelerated model provides a quantitative link between accelerated tests and service conditions and can be used to predict surface morphology-related parameters of static seals. When coupled with a morphology–leakage relationship, it further provides a theoretical basis for estimating seal leakage tendency.

**Author Contributions:** Conceptualization, B.Y. and H.J.; methodology, B.Y.; software, X.D.; validation, BY.; formal analysis, B.Y.; investigation, Y.L.; resources, W.L.; data curation, B.Y.; writing—original draft preparation, B.Y.; writing—review and editing, B.Y.; visualization, B.Y.; supervision, W.L.; project administration, X.D.; funding acquisition, X.D. All authors have read and agreed to the published version of the manuscript.

**Funding:** This research received no external funding.

**Institutional Review Board Statement:** Not applicable.

**Informed Consent Statement:** Not applicable.

**Data Availability Statement:** The raw data supporting the conclusions of this article will be made available by the authors on request.

**Conflicts of Interest:** The authors declare no conflicts of interest.

## References

1. Kim, G.H.; Lee, Y.S.; Yang, H.L. Experimental verification of newly proposed design of metal O-ring seal. *Vacuum* **2021**, *184*, 109942. [CrossRef]
2. Shen, M.; Xie, L.; Zhao, L.; Li, X.; Wang, Y.; Peng, X. Sealing characteristics of O-ring of Inconel 718 alloy in reaction pressure vessel. *J. Shanghai Jiaotong Univ.* **2015**, *49*, 1785–1791.
3. Li, X.; Hang, J.; Wei, S.; Cai, R.; Tan, Y.; Fan, H.; Li, J.; Li, Y. Manufacture of O-ring for reaction pressure vessels. *Press. Vessel Technol.* **2016**, *33*, 1–8.
4. Qiao, L.; Keller, C.; Zencker, U.; Völzke, H. Three-dimensional finite element analysis of O-ring metal seals considering varying material properties and different seal diameters. *Int. J. Press. Vessels Pip.* **2019**, *176*, 103953. [CrossRef]
5. Fantetti, A.; Tamatam, L.R.; Volvert, M.; Lawal, I.; Liu, L.; Salles, L.; Brake, M.R.W.; Schwingshackl, C.W.; Nowell, D. The impact of fretting wear on structural dynamics: Experiment and Simulation. *Tribol. Int.* **2019**, *138*, 111–124. [CrossRef]
6. Lai, P.; Gao, X.; Tang, L.; Guo, X.; Zhang, L. Effect of temperature on fretting wear behavior and mechanism of alloy 690 in water. *Nucl. Eng. Des.* **2018**, *327*, 51–60. [CrossRef]
7. Ming, H.; Liu, X.; Zhang, Z.; Wang, J.; Han, E.-H. Effect of normal force on the fretting wear behavior of Inconel 690 TT against 304 stainless steel in simulated secondary water of pressurized water reactor. *Tribol. Int.* **2018**, *126*, 133–143. [CrossRef]
8. Pei, W.; Zhang, S.; Ma, M.; Tan, W.; Zhu, G. Effect of work-rate on synergy of corrosion and wear of nickel-based 690 alloys under fretting conditions. *Results Eng.* **2025**, *26*, 104902. [CrossRef]
9. Wang, J.; Lei, Y.-j.; Li, Z.-y.; Li, H.-j.; Ren, Q.-y.; Jiao, Y.-j.; Cai, Z.-b. Effect of contact misalignment on fretting wear behavior between fuel cladding and Zr-4 grid. *Tribol. Int.* **2023**, *181*, 108299. [CrossRef]
10. Helmi Attia, M. Fretting fatigue and wear damage of structural components in nuclear power stations—Fitness for service and life management perspective. *Tribol. Int.* **2006**, *39*, 1294–1304. [CrossRef]

11. Chung, I.; Lee, M. An experimental study on fretting wear behavior of cross-contacting Inconel 690 tubes. *Nucl. Eng. Des.* **2011**, *241*, 4103–4110. [CrossRef]
12. Yun, J.Y.; Park, M.C.; Shin, G.S.; Heo, J.H.; Kim, D.I.; Kim, S.J. Effects of amplitude and frequency on the wear mode change of Inconel 690 SG tube mated with SUS 409. *Wear* **2014**, *313*, 83–88. [CrossRef]
13. Mi, X.; Bai, X.M.; Tang, P.; Xie, H.; Peng, J.F.; Zhu, M.H. The role of the third body in the fretting wear of 690 alloy. *Int. J. Mod. Phys. B* **2020**, *34*, 2050077. [CrossRef]
14. Li, J.; Shen, H.; Liao, Y.; Wang, Y.; Jin, S.; Peng, Z.; Wang, K.; Ren, Q. Fretting wear mechanism of nuclear fuel cladding tube under different tangential displacement. *Nucl. Eng. Des.* **2024**, *429*, 113567. [CrossRef]
15. Lazarevic, S.; Lu, R.Y.; Favede, C.; Plint, G.; Blau, P.J.; Qu, J. Investigating grid-to-rod fretting wear of nuclear fuel claddings using a unique autoclave fretting rig. *Wear* **2018**, *412–413*, 30–37. [CrossRef]
16. Winter, T.C.; Neu, R.W.; Singh, P.M.; Kolaya, L.E.; Deo, C.S. Fretting wear comparison of cladding materials for reactor fuel cladding application. *J. Nucl. Mater.* **2018**, *508*, 505–515. [CrossRef]
17. Blau, P.J. A multi-stage wear model for grid-to-rod fretting of nuclear fuel rods. *Wear* **2014**, *313*, 89–96. [CrossRef]
18. Zhang, W.; Lin, H.; Tao, J.; Bian, C.; Hu, M.; Xu, F.; Xie, L. Frictional wear characteristics of nickel-based alloy and reactor material in pressure vessel reactor. *Kerntechnik* **2022**, *87*, 278–286. [CrossRef]
19. Zhang, D.W.; Yang, G.C.; Lv, S.C.; Tian, C.; Li, Z.J. Fretting behavior of static metal seal and testing apparatus for fretting friction with low/high temperature. *Tribol. Int.* **2023**, *187*, 108676. [CrossRef]
20. Wang, B.; Zheng, M.; Zhang, W. Analysis and Prediction of Wear Performance of Different Topography Surface. *Materials* **2020**, *13*, 5056. [CrossRef]
21. Hao, D.; Gu, Y. Application of similarity criteria in the study of friction and wear on mechanical face seal. *J. China Univ. Pet. (Ed. Nat. Sci.)* **1990**, *14*, 61–67.
22. Wei, L.; Gu, B.; Zhang, P. Wear prediction for end face of contact mechanical seals. *J. Nanjing Univ. Technol. (Nat. Sci. Ed.)* **2012**, *34*, 16–21.
23. Sun, J.; Wei, L.; Feng, X.; Gu, B. Leakage Prediction Method for Contacting Mechanical Seals with Parallel Faces. *Chin. J. Mech. Eng.* **2010**, *23*, 7–15. [CrossRef]
24. Yu, Q.; Sun, J.; Yu, B.; Ma, C. A Fractal Model of Mechanical Seal Surfaces Based on Accelerating Experiment. *Tribol. Trans.* **2017**, *60*, 313–323. [CrossRef]
25. Sun, J. Research on the Prediction Theory of Mechanical Seal Leakage and Its Application. Doctoral Dissertation, Nanjing Tech University, Nanjing, China, 2006.
26. Zhang, Z.; Ding, X.; Xu, J.; Jiang, H.; Li, N.; Si, J. A study on building and testing fractal model for predicting end face wear of Aeroengine's floating ring seal. *Wear* **2023**, *532*, 205079. [CrossRef]


**Disclaimer/Publisher's Note:** The statements, opinions and data contained in all publications are solely those of the individual author(s) and contributor(s) and not of MDPI and/or the editor(s). MDPI and/or the editor(s) disclaim responsibility for any injury to people or property resulting from any ideas, methods, instructions or products referred to in the content.